Eur. Phys. J. Plus (2013) **128**: 44
DOI 10.1140/epjp/i2013-13044-x

THE EUROPEAN PHYSICAL JOURNAL PLUS

Regular Article

Performance of the ALICE Time-Of-Flight detector at the LHC

A. Akindinov[1], A. Alici[3,7], A. Agostinelli[2,3], P. Antonioli[3], S. Arcelli[2,3], M. Basile[2,3], F. Bellini[2,3], G. Cara Romeo[3], L. Cifarelli[2,3,7], F. Cindolo[3], M. Colocci[2,3], A. De Caro[5,7], D. De Gruttola[5,7], S. De Pasquale[5], K. Doroud[6], M. Fusco Girard[5], B. Guerzoni[2,3], D. Hatzifotiadou[3], D.W. Kim[4], J.S. Kim[4], S. Kiselev[1], S.C. Lee[4], D. Malkevich[1], A. Margotti[3], R. Nania[3,a], A. Nedosekin[1], F. Noferini[3,7], P. Pagano[5], A. Pesci[3], O. Pinazza[3], R. Preghenella[3,7], E. Scapparone[3], G. Scioli[2,3], K. Voloshin[1], M.C.S. Williams[3], C. Zampolli[3], and A. Zichichi[2,3,7]

[1] Institute for Theoretical and Experimental Physics, Moscow, Russia
RFBR grant 08-02-91911-CERNa
[2] Dipartimento di Fisica e Astronomia, Università degli Studi di Bologna, Bologna, Italy
[3] INFN, Sezione di Bologna, Bologna, Italy
[4] Department of Physics, Gangneung-Wonju National University, Gangneung, Republic of Korea
[5] Dipartimento di Fisica, Università di Salerno, and INFN, Sezione di Salerno, Salerno, Italy
[6] World Laboratory, Geneva, Switzerland
[7] Museo Storico della Fisica e Centro Studi e Ricerche "Enrico Fermi", Roma, Italy

Received: 18 March 2013
Published online: 23 April 2013 –

Abstract. The Time-Of-Flight (TOF) detector of the ALICE experiment at the CERN LHC is based on Multi-gap Resistive Plate Chambers (MRPCs) technology. During the 2009–2013 data taking the TOF system had very stable operations with a total time resolution of 80 ps. Details of the different calibration procedures and performance with data from collisions at the LHC will be described.

1 Introduction

The ALICE experiment at the LHC is studying the properties of the strongly interacting matter at very high temperature that is created in high-energy ion-ion collisions. This state of matter, the Quark-Gluon Plasma (QGP), gives us invaluable insight into the Quark-Gluon Coloured World, allowing to study fundamental aspects of our understanding of the Quantum Chromodynamics.

The ALICE experiment has collected data since 2009 with pp interactions at $\sqrt{s_{pp}} = 0.9$, 2.76, 7 and 8 TeV, with Pb-Pb at $\sqrt{s_{NN}} = 2.76$ TeV and with p-Pb at $\sqrt{s_{pN}} = 5.02$ TeV. The experiment [1–3] is characterized by extremely good tracking and Particle IDentification (PID) capabilities. Precise tracking is achieved down to 0.15 GeV/c through its Inner Tracking System (ITS) based on silicon detectors and the Time Projection Chamber (TPC). High-performance PID is accomplished taking advantage of the dE/dx measurements (ITS and TPC), a large-area Time of Flight (TOF), a Transition Radiation Detector (TRD) and a Cherenkov ring detector (HMPID). A dedicated quartz radiator Cherenkov detector (T0) provides a measurement of the event time of the collision.

The Time-Of-Flight (TOF) system [4] in ALICE is made of 1593 glass Multi-gap Resistive Plate Chamber (MRPC) detectors [5], each with a sensitive area of $7.4 \times 120\,\mathrm{cm}^2$. The TOF covers the pseudorapidity interval $[-0.9, +0.9]$ and the full azimuthal angle, for a total active area of 141 m^2. Each MRPC is segmented into 96 readout pads of area $2.5 \times 3.5\,\mathrm{cm}^2$, for a total of 152928 channels.

Test beam results may be found in [6] and [7], where the time resolution of a sample of MRPCs has been measured to be better than 50 ps, including the jitter contribution of the electronics. The TOF construction and detector assembly are described in details in [7], while the commissioning of the detector is reported in [8] and [9] with first results obtained with cosmic rays.

In this paper the TOF performance during the pp, the Pb-Pb and the p-Pb data taking at the LHC is described in detail.

[a] e-mail: nania@bo.infn.it

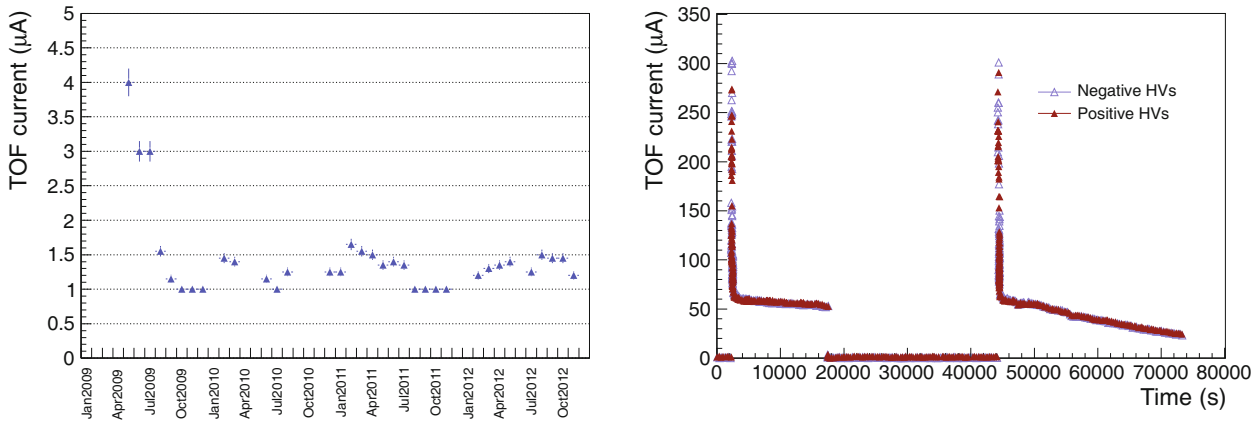

Fig. 1. Left: the TOF current without circulating beams as a function of time. Right: the TOF current for positive and negative high voltage as a function of time for two different fills in pp collisions.

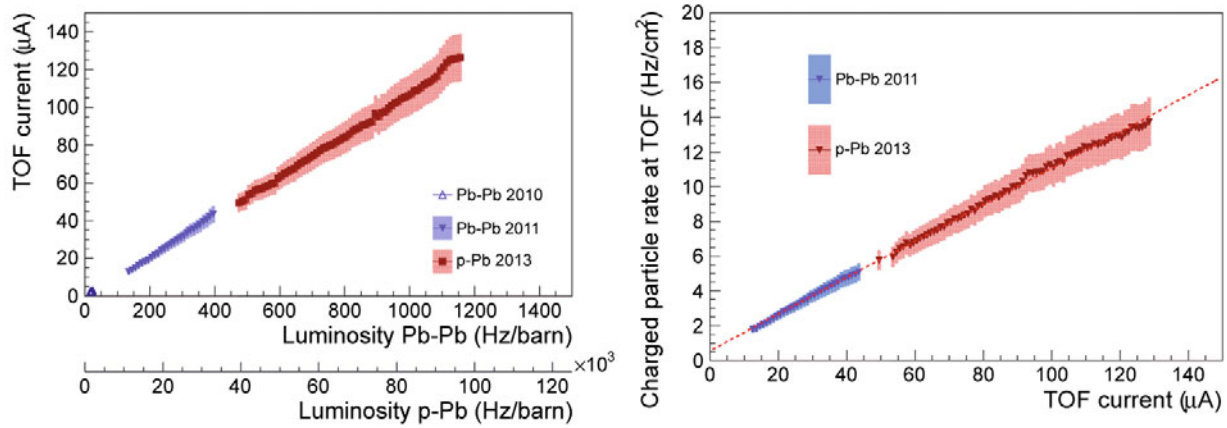

Fig. 2. Left: the TOF current *versus* luminosity in Pb-Pb and p-Pb. Right: the TOF estimated rate *versus* HV current. In both figures the points and the bands indicate the average and the spread of the measurements, respectively. The dashed line is the linear fit to the 2013 data.

2 MRPCs behaviour with cosmic rays and collisions

In the MRPCs the HV is applied with symmetric positive and negative values (±6500 V): the TOF current is defined as the sum over all MRPCs of the average of the two currents (positive and negative) and represents the total current flowing across the MRPCs.

The performance of the MRPCs was very stable along the first three years of the LHC operation. The TOF current as a function of time, during periods without circulating beams, is shown in fig. 1-left, indicating an initial MRPCs HV conditioning followed by stable operation with an average current per MRPC of few nA. The typical behaviour during the periods with beam is shown in fig. 1-right with the current increasing when the HV is switched on and then rapidly decreasing to a stable value which however depends on the beam conditions and luminosity. It was not necessary to adjust the applied high voltage during the three years of operation. The current of the MRPCs increased linearly with the LHC luminosity (fig. 2-left), with no sign of deviations related to the occurrence of abnormal noise current. The two horizontal axis are aligned to the same detector load considering the average track multiplicity and the ALICE interaction rate.

Considering the interaction rate at ALICE and the TOF hit multiplicity per event it is possible to estimate the average rate of particles in the detector as a function of the TOF current. The calculation is shown in fig. 2-right and it indicates a maximum average TOF rate of $\approx 14\,\mathrm{Hz/cm^2}$. Considering the two plots in fig. 2 it is possible to extrapolate the TOF rate to the luminosity foreseen in the ALICE upgrade beyond 2018 (5000 Hz/barn [10]). The expected rates will be $60\,\mathrm{Hz/cm^2}$: when compared to test beam results [11], this value indicates that also in the high-luminosity LHC period the MRPCs are expected to operate without loss in performance. From fig. 2-right it is possible to compute an average induced charge of $\approx 6\,\mathrm{pC}$ per track. This value is slightly higher than what obtained in test-beam [12], but still compatible considering that in ALICE the particles are of different species and cross the MRPC at different angles and with different momentum spectra. This low charge ensures a good rate capability and a slower ageing of the detector.

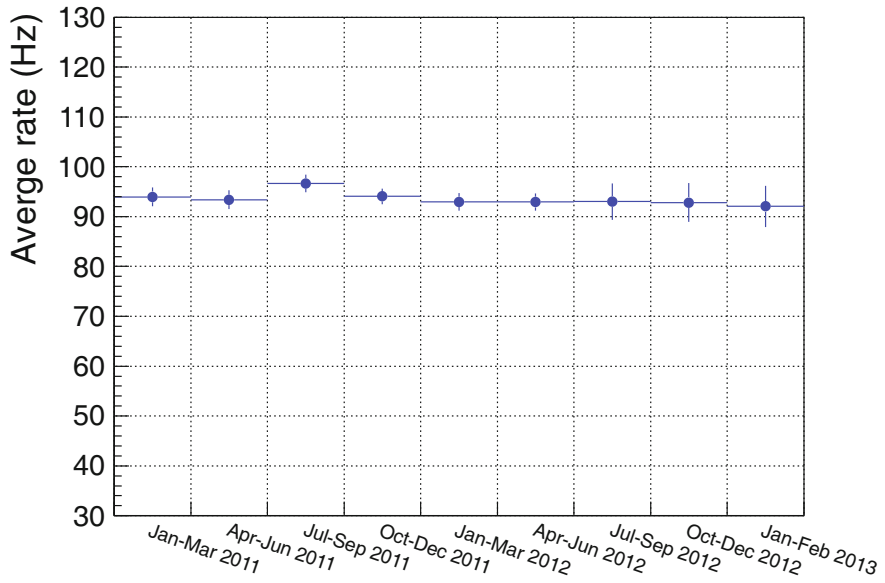

Fig. 3. Average rate (over three months) for the TOF cosmic trigger as a function of time.

3 TOF cosmic and collision trigger

Taking advantage of its large coverage, fine granularity and fast signals, the TOF system has been extensively used as a trigger detector during different periods of the ALICE commissioning and data taking. The fine granularity of the TOF and the relatively low noise of the MRPCs ($\approx 0.5\,\mathrm{Hz/pad}$ without beam) allowed triggering in several configurations, like back-to-back patterns in cosmic events or decays from resonances produced in Ultra-Peripheral Collisions (UPC).

The TOF trigger [13] consists of 1690 trigger channels, each covering $888\,\mathrm{cm}^2$ (equivalent to two half-MRPCs). The information coming from the front-end electronics is sent to the Local Trigger Modules (LTM) that are used as an interface between the front-end cards and the trigger board, called Cosmic and Topology Trigger Module (CTTM). The CTTM processes the signals and sends the result (within 800 ns after the collision) to the Central Trigger Processor (CTP) which provides the level-zero trigger (L0) for the experiment.

The trigger used to select cosmic events is based on a simple event topology [9]: a trigger is delivered when there is a back-to-back coincidence between two sectors in the azimuthal plane. In order to increase the acceptance for low-momentum muons, this condition is relaxed allowing the trigger to fire also if one out of the three sectors on each side of the lower one has fired. The purity of the trigger was estimated measuring the in-gate and out-of-gate rates [9] and was found to be 45%. This result is fully consistent with the offline data analysis where a cosmic muon track is found in $\approx 30\%$ of events. The rate has been very stable in time (fig. 3), allowing to collect hundreds of millions of muons to be used for TOF and other detectors calibration and for cosmic rays physics.

The TOF trigger was also used to select resonance decays in UPC during the Pb-Pb data taking in 2010 and 2011 and for p-Pb collisions in 2013. These events are characterized by the presence of just few tracks coming from resonance decays (ρ, ϕ or J/ψ) and almost no other tracks in ALICE. The main task of the TOF trigger was the selection of such topologies requesting that only few tracks reached the detector. Thanks to the available segmentation it was possible to require a small number of fired TOF pads (between 2 and 10) with an additional azimuthal topological cut (at least two opposite hits with $150^\circ < \Delta\phi < 180^\circ$).

4 TOF and MRPC efficiency

The TOF matching efficiency is defined as the ratio of the tracks matched by the TOF to those reconstructed using the ALICE tracking detectors, *i.e.* ITS, TPC and TRD. This quantity is obviously affected by the MRPC detection efficiency but also by the TOF geometrical acceptance, by hardware data taking conditions, by uncertainties in the track extrapolation, by the materials located in front of the TOF and by the track-TOF matching algorithm efficiency. Moreover tracks with $p_{\mathrm{T}} < 0.3\,\mathrm{GeV}/c$ do not reach the TOF detector due to the curvature of the trajectory in the magnetic field. For $p_{\mathrm{T}} > 0.3\,\mathrm{GeV}/c$ the matching efficiency rapidly increases until it saturates for $p_{\mathrm{T}} > 1\,\mathrm{GeV}/c$. A typical behaviour of the TOF matching efficiency is shown in fig. 4-left.

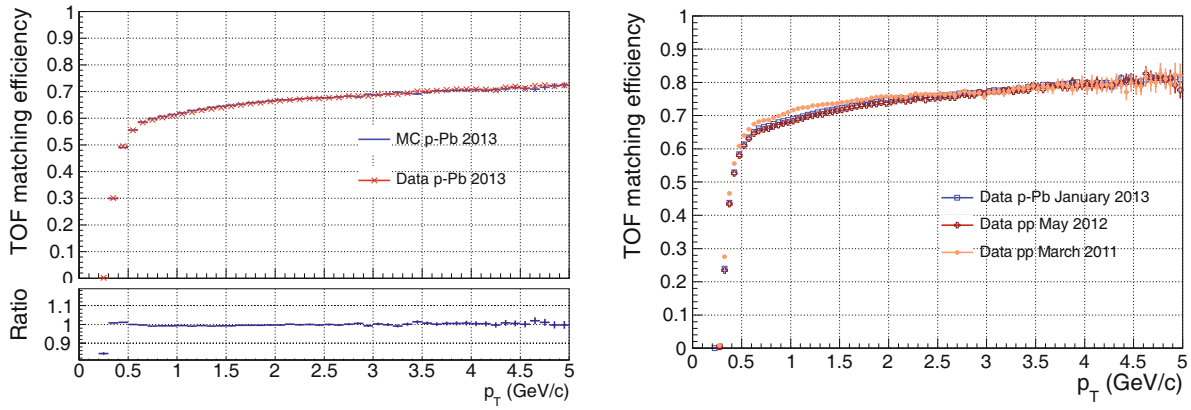

Fig. 4. Left: comparison between the TOF matching efficiency measured in 2013 p-Pb data and the one extracted from the corresponding simulation (top) and their ratio (bottom). Right: comparison between the TOF matching efficiency measured with 2011, 2012 pp data and with 2013 p-Pb data.

In fig. 4-left the matching efficiency measured in the 2013 p-Pb data is also compared with the one simulated in the corresponding Monte Carlo production. The Monte Carlo simulation takes into account the variations in the ALICE and TOF run conditions during the data taking. The tracking and the matching algorithms are common to both data and simulated events. The response of the MRPC detector as a function of the track impact point on the pad has been carefully simulated in the Monte Carlo according to a parametrization extracted from test beam results [6]. The MRPC efficiency in the centre of a pad is taken to be $\sim 99.5\%$. Due to the readout structure of the MRPC, a particle crossing the MRPC close to a pad boundary induces a charge on the pad and a smaller charge also on the neighbouring pad(s). The border between two pads is defined as a 13 mm wide region where the pad efficiency decreases going towards the neighbour pad (from 99.5% to zero), while the efficiency of the nearby pad correspondingly increases (from zero up to 99.5%). This effect concerns three sides of each pad. Along the fourth side (which has no neighbouring pad) there is only a 4 mm wide region where the efficiency slightly decreases, dropping to 88.3% at the pad edge. In the Monte Carlo program, these effects are included by means of a two-dimensional parametrized efficiency function obtained combining beam-test scans across and along the MRPC. With this procedure, the overall simulated MRPC detection efficiency is sligthly reduced to $\sim 98.5\%$. In fig. 4-left the agreement between data and Monte Carlo simulation is within 1%, confirming that the current simulation of the overall MRPC detection efficiency is realistic.

The matching efficiency for tracks with $p_{\mathrm{T}} > 2.0\,\mathrm{GeV}/c$ has been stable throughout the years, as shown in fig. 4-right. For $p_{\mathrm{T}} < 2.0\,\mathrm{GeV}/c$ the matching efficiency slightly varies due to a different number of TRD sectors installed at different times in front of the TOF: their contribution to the material budget and the presence or not of their position information affect the global tracking in ALICE and also the TOF matching efficiency.

5 Calibrations and PID analysis

5.1 Timing calibration and performance

The TOF time calibration is based on the determination of three components: i) a global offset, which is common to all the channels, ii) a channel-by-channel offset, which depends on the channel and iii) a time-slewing correction at the channel level. All the three calibrations require full track reconstruction in the ALICE detector and, as a consequence, rely on the calibration of the main tracking device, the TPC [14], which also provides the momentum information.

The need to sample in time the global offset comes from the observation of a time shift in the LHC clock phase, which results in a non constant offset in the measured time of flight. This shift is due to the temperature dependence of the fiber refractive index, which affects the LHC clock time distributed to the experiments. The global offset is derived from a time sampling of the TOF data, using only particles with a reconstructed momentum $p > 0.5\,\mathrm{GeV}/c$ to assure a good tracking performance almost independent of the momentum. The measured arrival times of flight are compared to the expected times obtained from the measured track length and momentum in the pion mass hypothesis. The choice to use the pion mass as reference is driven by the fact that pions are the most abundant species produced in the collisions and they largely dominate the time distribution. The difference between the measured times of flight and the expected times is sampled in time (10 minute samples) for all tracks and the corresponding distribution is fitted with a Gaussian function whose mean corresponds to the global channel offset for the time interval under study (fig. 5-left).

The channel-by-channel offset calibration accounts for the delays introduced in the measured times of flight by the cable lengths and by the electronics. Such calibration is carried out as for the global offset, but in this case the distribution of the differences between the measured and expected times is evaluated for every channel. Again, a Gaussian fit is performed for each distribution and its mean value gives the channel-by-channel offset. It is clear that a much larger statistics is needed to perform such a calibration, due to the fact that a minimum number of tracks

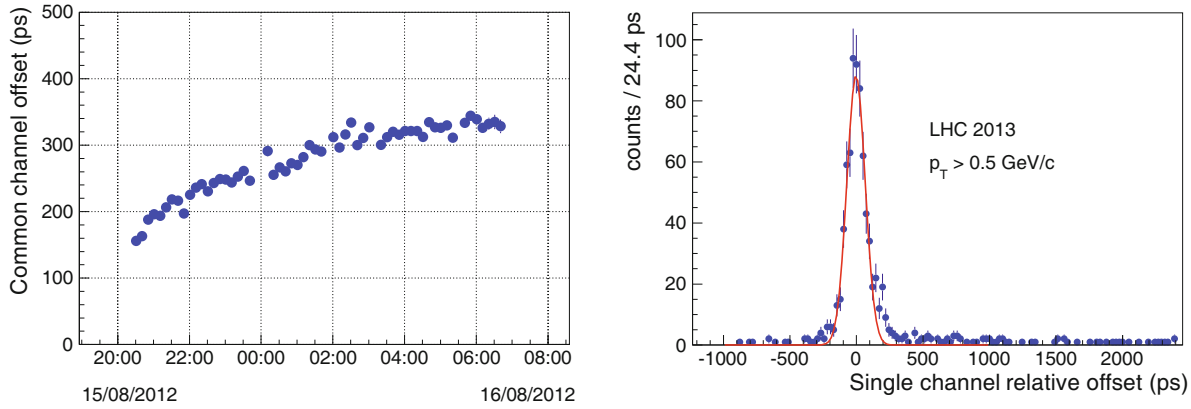

Fig. 5. Left: common global offset as a function of time as measured in one LHC fill in 2012. Right: an example of a calibration fit used to extract the single-channel offset.

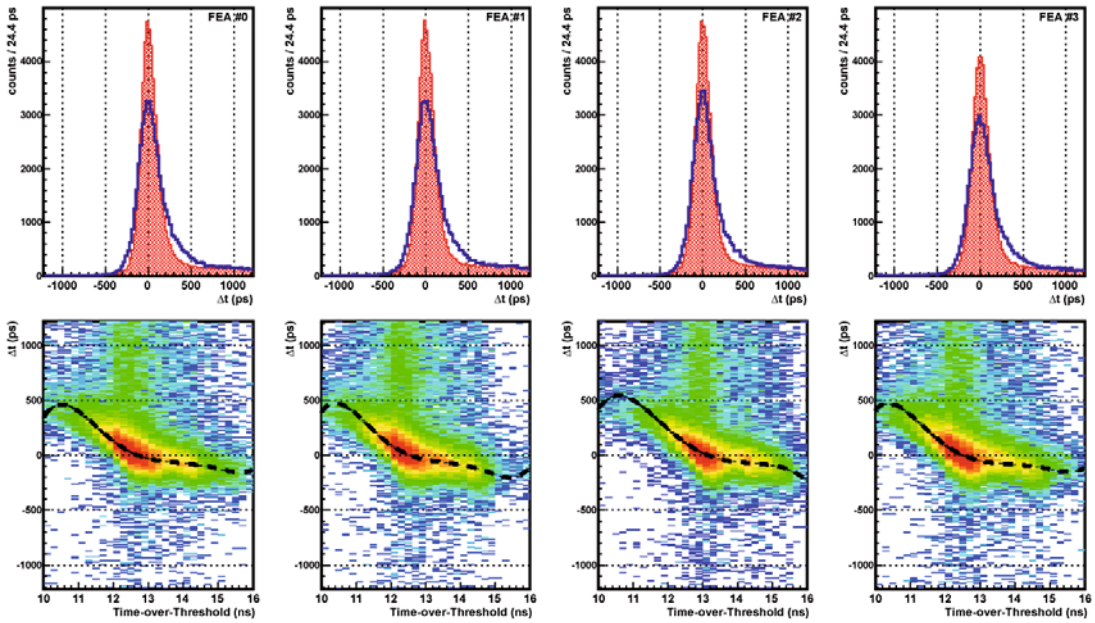

Fig. 6. Example of time-slewing calibration shown for 4 front-end cards of a MRPC. Data correspond to Pb-Pb collisions and the tracks are selected in the range $0.5 < p < 1.5\,\mathrm{GeV}/c$. Top: the empty and shaded histograms show the signal before and after time-slewing correction. Bottom: time-amplitude (measured as Time-over-Threshold) correlation. The dashed lines show the polynomial function used for the final correction.

per channel is required to assure a reliable fit. Several million events are used for pp collisions, collected over several days of data taking. This integration in time is allowed by the absence of significant changes in the channel-by-channel delay, as observed over a long period of data taking. Obviously, in the case of Pb-Pb or p-Pb data, the number of events used for this calibration decreases considerably, due to the much larger average number of particles per event. An example is shown in the right panel of fig. 5. The calibration is repeated at regular time intervals in order to properly consider possible modifications of the TOF hardware configuration.

Finally, the time-slewing effect correction is applied. The correction makes use of the correlation between the measured time and the signal width (Time-over-Threshold, ToT), corresponding to the time interval during which the signal released by TOF remains over the threshold of the signal discriminator[1]. The time slewing calibration is a channel-by-channel calibration. To reach the very high statistics necessary for this two-dimensional calibration, data are collected over very long periods (several months) or at every hardware intervention on the TOF: also in this case tests have shown no significant changes with time, as expected from the stable operations of the MRPCs and of the

[1] In the TOF readout electronics [15,16] the Front-End ASICs (NINO) amplifies and discriminates the MRPC signal with an output width correlated to the charge of the input signal. The measured time of flight is given by the time when the signal becomes larger than the threshold (*leading edge*). The time when the signal becomes smaller than the threshold defines the *trailing edge*. The ToT corresponds to the time difference between the *leading* and the *trailing* edges and it is correlated to the MRPC charge.

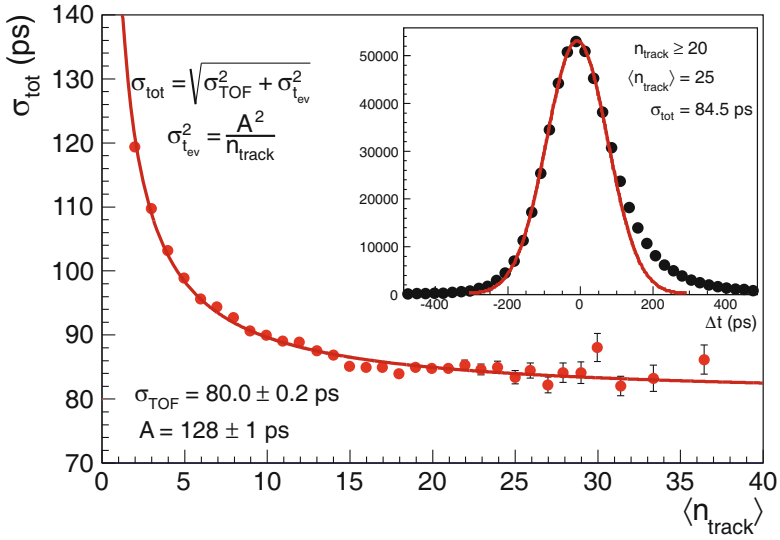

Fig. 7. Total time resolution for pion tracks on TOF with $0.95 < p < 1.05\,\mathrm{GeV}/c$ as a function of the number of tracks used to define the TOF event time. Data refer to p-Pb collisions. The inset shows the original distribution for a track multiplicity on TOF > 20 which corresponds to an average of 25.

readout electronics. The correlation between the measured times and the ToT is fitted with a 5th-order polynomial (fig. 6-bottom) and the improvement after this calibration step is demonstrated in fig. 6-top. The data refer to Pb-Pb collisions and the effect of the wide momentum interval used for this calibration and the mismatch rate in such high-multiplicity events is visible as a tail on the right-hand side of the upper plots and in the green bands excess in the bottom plots. The fit parameters are then used to obtain the correction to the measured times according to their ToT.

After the above three calibrations, it is possible to evaluate the TOF performance in terms of time resolution. For tracks with a momentum in the range $0.95 < p < 1.05\,\mathrm{GeV}/c$ the difference between the measured time of flight and the pion time expectation is computed. The distribution is fitted with a Gaussian function, whose width is the convolution of the TOF time resolution σ_{TOF} and the event time (that is the collision time) resolution $\sigma_{t_{ev}}$: $\sigma^2_{\mathrm{tot}} = \sigma^2_{\mathrm{TOF}} + \sigma^2_{t_{ev}}$. The contribution from tracking (see sect. 5.3) is negligible for the momentum range considered. For the event time the one measured by the TOF itself is used as described in sect. 5.2. Since the TOF t_{ev} resolution is expected to scale with the square root of the number of tracks used ($\sigma_{t_{ev}} = \frac{A}{\sqrt{n_{\mathrm{tracks}}}}$), the measured σ_{tot} can be plotted *versus* n_{tracks} and fitted according to this expression. Figure 7, obtained for p-Pb collisions, reports the result of such fit indicating for $n_{\mathrm{tracks}} \to \infty$ a value corresponding to a TOF time resolution of 80 ps. The inset shows an example of a Gaussian fit for a track multiplicity on TOF in excess of 20: the distribution has a tail on the right, which was not observed during test beams, and might be related to residual miscalibrations which are currently under investigation. Notice that, for example, no time walk effect due to the position of the track inside a readout pad has been up to now considered. The excess observed in fig. 6 is much reduced in fig. 7 because of the narrower momentum range used and of the lower mismatch probablity in p-Pb events. The Gaussian fit in the inset is performed in the range between -160 and 80 ps; the inclusion of the right-hand side tail would worsen the result by $\approx 10\%$.

5.2 Event time determination with the TOF

The TOF PID strategy is based on a time difference between the arrival time measured by the TOF and the event time which is estimated event by event. In ALICE the T0 detector is dedicated to such a measurement [17]: it is composed of two rings of quartz Cherenkov counters placed close to the beam direction in the forward rapidity regions (both sides). However, due to the detector acceptance, expecially in pp collisions, no signals are observed by the T0 for a fraction of the events and, as a consequence, an estimate of the event time is not available from the detector. For these events the uncertainty in establishing the event time depends on the finite size of the bunches and it varies between 80 and 200 ps with respect to the nominal time signal from the LHC: this uncertainty contributes in a significant way to the observed overall time of flight resolution σ_{tot}.

In order to reduce this contribution an alternative method was developed where the TOF information itself is used to determine the event time when at least three tracks have an associated TOF signal. This is done by means of a combinatorial algorithm which compares the measured TOF times to the expected times of the tracks, assuming a common event time t_{ev}. This latter quantity is obtained from a χ^2-minimization procedure. In detail, for a given

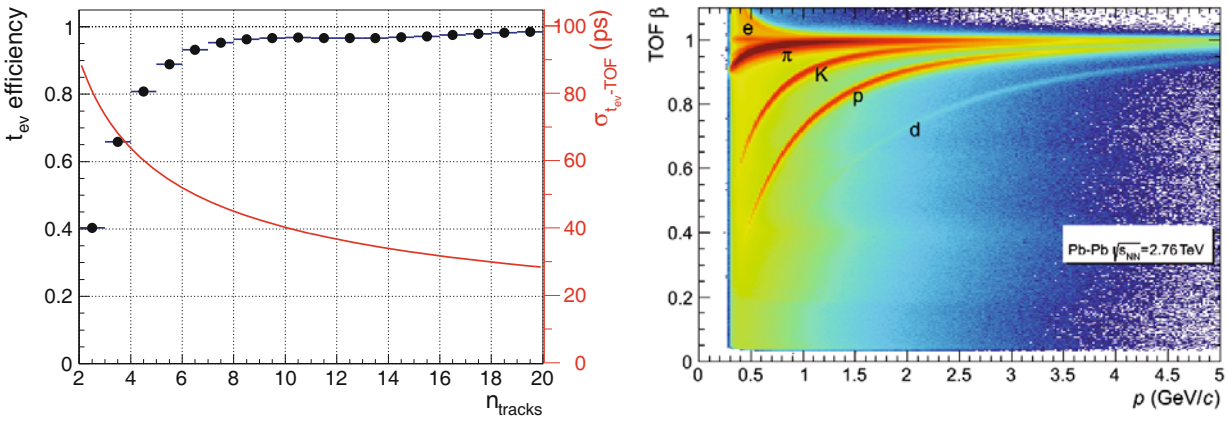

Fig. 8. Left: efficiency and time resolution for the TOF-based event time algorithm as a function of the number of tracks matched to TOF and available for the computation. Right: correlation $\beta = v/c$ *versus* momentum as observed by TOF in Pb-Pb collisions after the calibration procedures.

track j, the event time is determined using all the other tracks in the event and evaluating the following χ^2 expression for all possible combinations of masses ($m_i, i = \pi$, K, p),

$$\chi^2 = \sum_{n_{\rm tracks}} \frac{((t_{\rm TOF} - t_{ev}) - t_{\rm exp}(m_i))^2}{\sigma^2_{\rm TOF} + \sigma^2_{t_{\rm exp}}}, \tag{1}$$

where the sum is over all tracks matched at TOF other than j, $t_{\rm TOF}$ is the track measured time and $t_{\rm exp}$ is the expected time with the mass hypothesis i. $\sigma_{\rm TOF}$ and $\sigma_{\rm t_{exp}}$ are the corresponding errors. The combination that minimises the χ^2 is used to derive t_{ev} which is then subtracted from the TOF time associated to track j. This procedure, which is repeated for each track in the event, ensures that the measured event time is always independent of the TOF measured time of the track, thus avoiding possible biases in the determination of t_{ev}. A check on the χ^2 value of each used track and of the final t_{ev} is also performed in order to reject tracks not consistent with the sample for any mass hypothesis (mismatched tracks) and eventually to reject also the event time: this implies a reduction in the efficiency of the algorithm.

In fig. 8-left the efficiency for the TOF event time algorithm is reported as a function of the number of TOF-matched tracks available for the computation. In order to reduce the computation time of the combinatorial algorithm when the number of TOF tracks is quite large, TOF tracks are grouped into samples of 10 (order of 10^3 combinations per sample) and the final t_{ev} is extracted by averaging the event time of all samples. This feature is responsible of a small structure in the efficiency between 10 and 13 tracks where the algorithm switches from 1 to 2 samples. In figs. 8-left and 7 the contribution to the total time resolution due to the t_{ev} as calculated with the TOF is reported, indicating that it becomes negligible when the number of tracks is high (≈ 25 ps at $n_{tracks} = 30$ and even lower resolutions for the high-multiplicity Pb-Pb collisions where events with low centrality (0–10%) have on average 600 particles on TOF).

In the physics analysis the event time is determined combining the t_{ev} estimated by the T0 detector and by the TOF tracks, weighted by the respective resolutions. For the small fraction of events where none of the two measurements is available the event time is taken as the average obtained during the run, of course with a much worse resolution on t_{ev}.

5.3 Particle Identification with TOF

The TOF performance obtained through the calibration and data analysis described in previous sections are first summarized in terms of the measured β-momentum correlation for tracks matching the TOF, as shown in fig. 8-right. In this figure pions, kaons and protons are clearly separated in the intermediate $p_{\rm T}$ range. Points corresponding to non physical values in the β-momentum plane are due to mismatched tracks at TOF, *e.g.*, hit registered at TOF but not associated to the true track. The amount of this background depends on the type of the collisions and it can be reduced at low momentum using the TPC $\mathrm{d}E/\mathrm{d}x$ information.

Analysing data with the TOF detector, the simplest PID estimator for a given mass hypothesis m_i ($i = e$, μ, π, K, p, d, t, ^{3}He, ^{4}He) is constructed as an n-σ quantity, assuming a Gaussian description of the response function of the detector, in the following way:

$$\hat{PID}_{{\rm TOF},i} = \frac{t_{\rm TOF} - t_{ev} - t_{\rm exp}(m_i, p, L)}{\sigma_{\rm tot}(p, m_i, t_{ev})}, \tag{2}$$

where $t_{\rm TOF}$ is the hit time measured by the TOF detector, t_{ev} is the event time of the collision and $t_{\rm exp}$ the expected time for a particle of mass m_i, momentum p and track length L reaching the TOF.

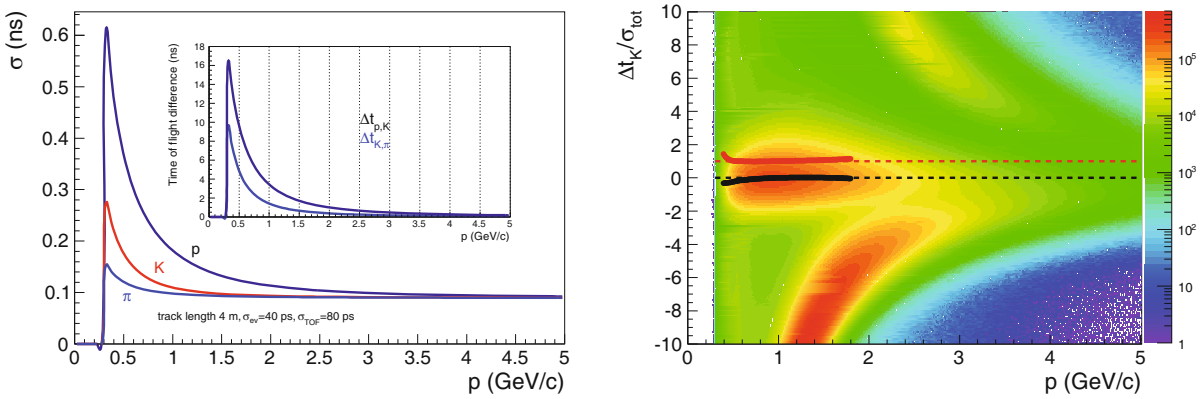

Fig. 9. Left: resolution function for PID as a function of momentum p for protons, kaons and pions assuming $\sigma_{\rm TOF} = 80\,$ps, $\sigma_{t_{ev}} = 40\,$ps and a 4 m track length. In the inset the expected Time-Of-Flight difference between protons and kaons and kaons and pions for a 4 m track length is also shown. Right: for real data, n-σ deviations *versus* the track momentum considering the kaon expected time. The accumulations corresponding to pions and protons are clearly visible. Points indicate average (black) and width (red) of the distribution for each momentum bin.

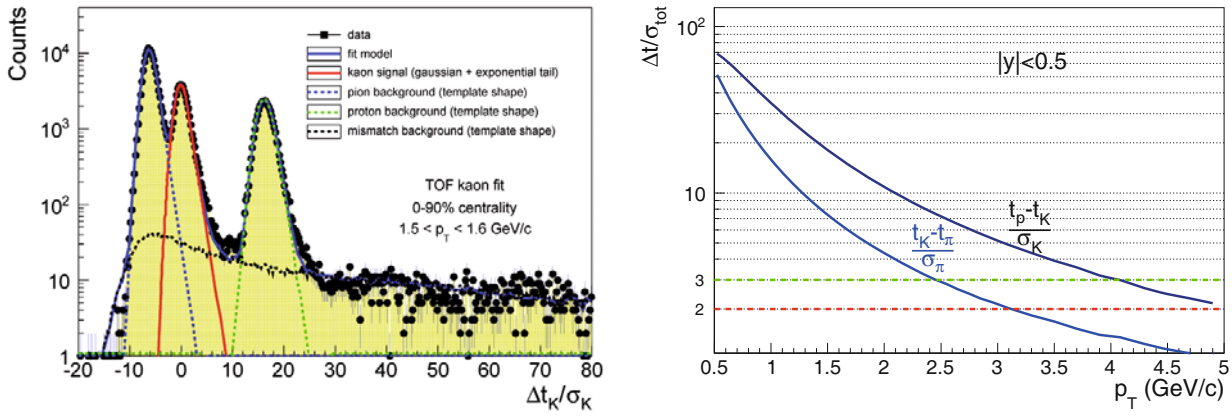

Fig. 10. Left: TOF kaon fit in Pb-Pb collisions at $\sqrt{s_{\rm NN}} = 2.76\,$TeV using the Gaussian unfolding technique in the momentum range $1.5 < p_{\rm T} < 1.6\,{\rm GeV}/c$. Right: the present separation power of the TOF for kaon-pion and proton-kaon as a function of $p_{\rm T}$.

The resolution function $\sigma_{\rm tot}(p, m_i, t_{ev})$ takes into account, summing quadratically, the intrinsic TOF detector contribution ($\sigma_{\rm TOF} \approx 80\,$ps as explained in sect. 5.1), the uncertainty on the event time of the collision (which depends on the method actually used in the given event, as discussed in sect. 5.2) and the uncertainty due to the tracking and reconstruction (including estimates of the energy losses through the material). The latter contribution has been parametrized as a function of the momentum on the basis of real data and using Monte Carlo simulations, as shown in fig. 9-left. In absolute terms this contribution becomes dominant at small momenta for heavier particles, but, on the other hand, the expected time difference increases much more, as shown in the insert of fig. 9-left.

The $\hat{PID}$ variable is then used to implement simple 2 or 3 σ cuts, depending on the requirements of the specific analysis. The good understanding of the detector response and parametrization of its resolution is confirmed by monitoring the average values (expected around zero) and pulls of the distribution of this variable (expected around 1). As an example, the distribution of this variable as a function of momentum for the kaon hypothesis is shown in fig. 9-right. Pions and protons are also visible as well as the region where pions start worsening the purity of a selected kaon sample. Each momentum slice has been fitted with a gaussian fit bound to $[-2, 2]$ values and the resulting mean and width of the distribution are plotted as black and red points. By construction the fitted width corresponds to the pull of the distribution of the $\hat{PID}$ variable. In the range where there is no contamination from pions the values are in nice agreement with the expected values for mean and pull of the variable (0 and 1, respectively, represented by the dashed lines) validating the description of the resolution function. Note that in PbPb at low $p_{\rm T}$ (below $400\,{\rm MeV}/c$) the presence of mismatched tracks alters the distribution, but this contribution can be removed using the TPC information.

The described Gaussian approach has been used for PID identification track by track in several ALICE analyses, including, for example, studies of charmed mesons [18], resonances [19], electron spectra [20]. PID analyses involving TOF are performed mainly in conjuction with the TPC detector, separately or combining directly the information of the two detectors.

A complementary approach has been developed summing over all events and fitting the cumulative distributions of the time difference with respect to a given hypothesis. This approach (Gaussian unfolding) has been used in particular to fit identified spectra [21]. An example for a given transverse momentum slide is shown in fig. 10-left.

The $P\hat{I}D$ estimator can be further used to construct a probability of identification for a given mass hypothesis via

$$P_i^{\mathrm{TOF}} = \frac{e^{-P\hat{I}D^2}}{\sqrt{2\pi\sigma_{\mathrm{tot}}}}. \tag{3}$$

This quantity can be used to select tracks above a given identification probability threshold similarly to what can be done by applying a cut on $P\hat{I}D$ at a specific value. However this approach allows to combine the PID capabilities of the different ALICE detectors within the Bayesian framework [2]. A full discussion of this method is beyond the scope of this paper and entails also the performance of the other PID detectors. It is nevertheless worth to note that this approach is now increasingly used in different ALICE analyses.

As a summary of the presented results, in fig. 10-right the separation power of the TOF for kaon-pion and proton-kaon as a function of p_{T} is shown. The separation is calculated as the distance between the peaks divided by the Gaussian width σ_{tot} of the pion or the kaon response, respectively. Usually this is shown as a function of total momentum p as in fig. 9-right; however, since most physics results are reported in transverse momentum bins, here the separation power in p_{T} bins is reported, averaging the momentum-dependent response over the range $|y| < 0.5$.

6 Conclusions

The ALICE TOF system, based on the MRPC detectors, has shown very stable operation during the first three years of colllisions at the LHC. Currents and rates behaved as expected during the periods of data taking with beam, with no sign of degradation of the detector, allowing also to use the TOF as a trigger detector. Using the ratio between TOF matched tracks with those reconstructed in the tracking detectors, the MRPC detection efficiency is found to be compatible with the 98.5% of the Monte Carlo simulations that rely on test beam results and this efficiency is stable in time. The data demonstrate a TOF global time resolution around 80 ps. In events with several particles reaching the TOF modules it is possible to use these tracks to define the event time of the collision with an accuracy of ≈ 25 ps at $n_{\mathrm{tracks}} = 30$ and even better for the high-multiplicity Pb-Pb collisions. Several approaches have been developed for particle identification with TOF, reaching a kaon-pion and proton-kaon three-σ separation up to p_{T} of 2.5 and 4.0 GeV/c, respectively.

We thank all colleagues from the ALICE Collaboration who made available some of the information used in the present paper, in particular the TPC and T0 groups. The ALICE Management, the Technical and Run Coordination, the DAQ, DCS, ECS, Trigger and Offline Groups are especially acknowledged for their help and support during the data taking period and the offline reconstruction of the events.

References

1. ALICE Collaboration, J. Phys. G: Nucl. Part. Phys. **30**, 1517 (2004).
2. ALICE Collaboration, J. Phys. G: Nucl. Part. Phys. **32**, 1295 (2006).
3. ALICE Collaboration, JINST **3**, S08002 (2008).
4. ALICE Collaboration, Addendum to TOF Technical Design Report CERN/LHCC 2002-016.
5. E. Cerron-Zeballos *et al.*, Nucl. Instrum. Methods A **374**, 132 (1996).
6. A. Akindinov *et al.*, Nucl. Instrum. Methods A **532**, 611 (2004).
7. A. Akindinov *et al.*, Nuovo Cimento B **124**, 235 (2009).
8. A. Akindinov *et al.*, Nucl. Instrum. Methods A **615**, 37 (2010).
9. A. Akindinov *et al.*, Eur. Phys. J. C **68**, 601 (2010).
10. ALICE Collaboration, CERN-LHCC-2012-012 / LHCC-I-022 September 7, 2012.
11. A. Akindinov *et al.*, Nucl. Instrum. Methods A **490**, 58 (2002).
12. A. Akindinov *et al.*, Eur. Phys. J. C **34**, 325 (2004).
13. A. Akindinov *et al.*, Nucl. Instrum. Methods A **602**, 372 (2009).
14. J. Alme *et al.*, Nucl. Instrum. Methods A **622**, 316 (2010).
15. F. Anghinolfi *et al.*, Nucl. Instrum. Methods A **533**, 183 (2004).
16. A. Akindinov *et al.*, Nucl. Instrum. Methods A **533**, 178 (2004).
17. A. Maevskaya *et al.*, Proc. Sci. ISHEEP **XXI**, 110 (2012).
18. ALICE Collaboration, JHEP **01**, 128 (2012).
19. ALICE Collaboration, Eur. Phys. J. C **72**, 2183 (2012).
20. ALICE Collaboration, Phys. Rev. D **86**, 112007 (2012).
21. ALICE Collaboration, Phys. Rev. Lett. **109**, 252302 (2012).